catalysts

MDPI

Article

Easily Recycled CuMgFe Catalysts Derived from Layered Double Hydroxides for Hydrogenolysis of Glycerol

Xiaopeng Yu [1,*], Fubao Zhang [2], Yi Wang [1] and Dejun Cheng [1]

[1] Department of Chemical Engineering, Sichuan University of Science and Engineering, Zigong 643000, China; yiwanghg@suse.edu.cn (Y.W.); sunshine80131515@suse.edu.cn (D.C.)
[2] Zhonghao Chenguang Research Institute of Chemical Industry Co. Ltd., Zigong 643201, China; zhangfubao@haohua.chemchina.com
* Correspondence: xiaopengyu@suse.edu.cn; Tel.: +86-813-5506-521

Abstract: A series of CuMgFe catalysts with different (Cu + Mg)/Fe molar ratios derived from hydrotalcites were prepared by coprecipitation for the hydrogenolysis of glycerol to 1,2-propanediol (1,2-PDO). X-ray diffraction (XRD), scanning electron microscopy (SEM), transmission electron microscopy (TEM), X-ray photoelectron spectra (XPS), vibrating sample magnetometer (VSM), hydrogen temperature-programmed reduction (H_2-TPR), CO_2-TPD, and H_2-TPD (temperature-programmed desorption of CO_2 and H_2) were used to investigate the physicochemical properties of the catalysts. The CuMgFe-layered double oxides (CuMgFe-4LDO) catalyst with (Cu + Mg)/Fe molar ratio of 4 exhibited superior activity and stability. The high glycerol conversion and 1,2-propanediol selectivity over CuMgFe-4LDO catalyst were attributed to its strong basicity, excellent H_2 activation ability, and an increase in the surface Cu content. The CuMgFe catalysts could be easily recycled with the assistance of an external magnetic field due to their magnetism.

Keywords: CuMgFe; layered double hydroxides; hydrogenolysis of glycerol; 1,2-propanediol; recycled

Citation: Yu, X.; Zhang, F.; Wang, Y.; Cheng, D. Easily Recycled CuMgFe Catalysts Derived from Layered Double Hydroxides for Hydrogenolysis of Glycerol. *Catalysts* **2021**, *11*, 232. https://doi.org/10.3390/catal11020232

Academic Editors: Juan Antonio Cecilia and Carmen Pilar Jiménez Gómez
Received: 20 January 2021
Accepted: 7 February 2021
Published: 9 February 2021

1. Introduction

Biodiesel is considered as a possible new pattern of renewable energy. Large-scale biodiesel production has brought about a surplus by-product of glycerol. Undoubtedly, the conversion of excess glycerol into higher-value chemicals can increase the economic value of the biodiesel industry. Different processes such as oxidation, dehydration, and hydrogenolysis have been proposed for the conversion of glycerol [1–5]. One of the attractive ways is hydrogenolysis to 1,2-propanediols (1,2-PDOs) because 1,2-PDO is widely used as a monomer for antifreeze agent, polyester resins, paints additive, liquid detergent, food, etc. Some results have been reported in selective catalytic hydrogenolysis of glycerol to 1,2-PDO [6–24].

Noble metals such as Rh, Ru and Pt are extensively used in the hydrogenolysis of glycerol owing to their high reactivity [9–15]. Nevertheless, these catalysts usually facilitate excessive C–C cleavage, resulting in a poor selectivity to 1,2-PDO. Cu-based catalysts exhibit high selectivity to 1,2-PDO in the hydrogenolysis of glycerol due to poor activity for C–C bond cleavage and high efficiency for C–O bond hydro-dehydrogenation. Cu–Cr [16], Cu/ZnO [17,18], Cu/Al_2O_3 [17,19], Cu/SiO_2 [20,21], Cu/MgO [22,23] catalysts have been reported by several groups. It has been demonstrated that the activity of Cu-based catalysts for hydrogenolysis of glycerol depends strongly on the dispersion and/or the surface area of exposed Cu [8,20,21]. Additionally, the acidity/basicity of Cu-based catalysts also plays an important role in the hydrogenolysis reaction of glycerol [22,24].

Layered double hydroxides (LDHs), also known as hydrotalcite-like compounds, are a class of anionic clay materials that allow the uniform mixing of different bivalent and trivalent cations. Thermal decomposition of LDHs leads to the formation of mixed oxides with small crystal size, basicity, high dispersion, and large specific surface area.

It has been reported that Cu-based catalysts derived from hydrotalcites are of basicity and dispersed copper particles [8,24–27], which could improve the catalytic performance in the hydrogenolysis of glycerol. Geng et al. [28] disclosed that the Cu–Ca–Al catalyst derived from hydrotalcite is more active and selective for the formation of propanediols. Nonetheless, these catalysts suffer from serious difficulties in the recovery and reuse from the perspective of ecological and economical sustainability. Magnetic catalysts can be easily separated by an external magnetic field, reducing the consumption of auxiliary substances, saving energy and time in separation, and bringing significant economic and environmental benefits. However, to the best of our knowledge, there is no detailed understanding of magnetic Cu-based catalysts derived from hydrotalcites in the hydrogenolysis of glycerol.

The aim of the present work is to develop easily recycled Cu-containing catalysts in the hydrogenolysis of glycerol. Magnetic CuMgFe mixed-oxide catalysts derived from hydrotalcites were prepared by coprecipitation, and the effect of (Cu + Mg)/Fe molar ratio on the activity of the catalysts was discussed in detail.

2. Results and Discussion

2.1. Characterization Results

2.1.1. Structure and Morphology of CuMgFe-xLDH and CuMgFe-xLDO

The XRD patterns of CuMgFe-xLDH are shown in Figure 1a. CuMgFe-2LDH, CuMgFe-3LDH, CuMgFe-4LDH, and CuMgFe-5LDH exhibited the characteristic reflections of hydrotalcite. Compared with CuMgFe-2LDH, the sharp diffraction peaks of CuMgFe-3LDH evidenced a better crystallization of the phase of hydrotalcite. Oppositely, CuMgFe-4LDH and CuMgFe-5LDH exhibited a lower crystallization with the increase of (Cu + Mg)/Fe molar ratio. Increasing (Cu + Mg)/Fe molar ratio might lead to the structural distortion and the orderliness decline of hydrotalcite.

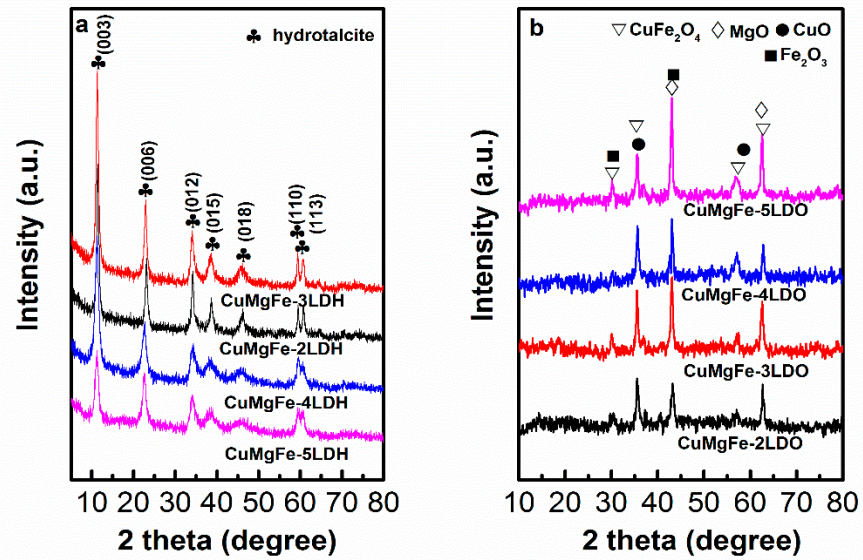

Figure 1. XRD patterns of (**a**) CuMgFe-xLDH and (**b**) CuMgFe-xLDO.

The XRD patterns of CuMgFe-xLDO catalysts with different (Cu + Mg)/Fe molar ratios are shown in Figure 1b. After calcination at 600 °C, all LDHs were transformed to mixed oxides and spinel phase. For all the CuMgFe-xLDO samples, the diffraction peaks at around 30.2°, 35.5°, 57.1°, and 62.7° corresponded to the (220), (311), (511), and (440) planes of $CuFe_2O_4$ spinel phase (JCPDS card no. 77-0010), respectively. Meanwhile, the CuO phase (at around 35.5° (002) and 58.3° (202)) also might be present, but its diffraction peaks were partially overlapped with those of $CuFe_2O_4$. Consequently, it was difficult to distinguish in the XRD results. The diffraction peaks at 30.3° and 43.3° could correspond to the (220) and (400) planes of the Fe_2O_3 phase (JCPDS card no. 39-1346), respectively.

Additionally, the diffraction peaks at 42.9° and 62.3° were also observed, which could be associated with the (200) and (220) planes of the MgO phase (JCPDS card no. 04-0829).

The morphology of CuMgFe-3LDH and CuMgFe-4LDH revealed by SEM is shown in Figure 2. CuMgFe-3LDH displayed a layered structure of solid lamellar (Figure 2A), whereas some solid lamellar structures accumulated obviously in CuMgFe-4LDH (Figure 2B). Figure 2C,D shows the images of CuMgFe-3LDH and CuMgFe-4LDH after calcination, which maintained the plate-like morphology of the original precursor. High resolution transmission electron microscope (HRTEM)was also used to reveal the structure of CuMgFe-4LDO sample. A typical HRTEM image of CuMgFe-4LDO showed two identified reflection patterns with interplanar distances of 0.253 nm and 0.205 nm (Figure 2E), corresponding to the (002) plane of CuO phase and (220) plane of $CuFe_2O_4$ phase [29,30], respectively, which was in line with the XRD results.

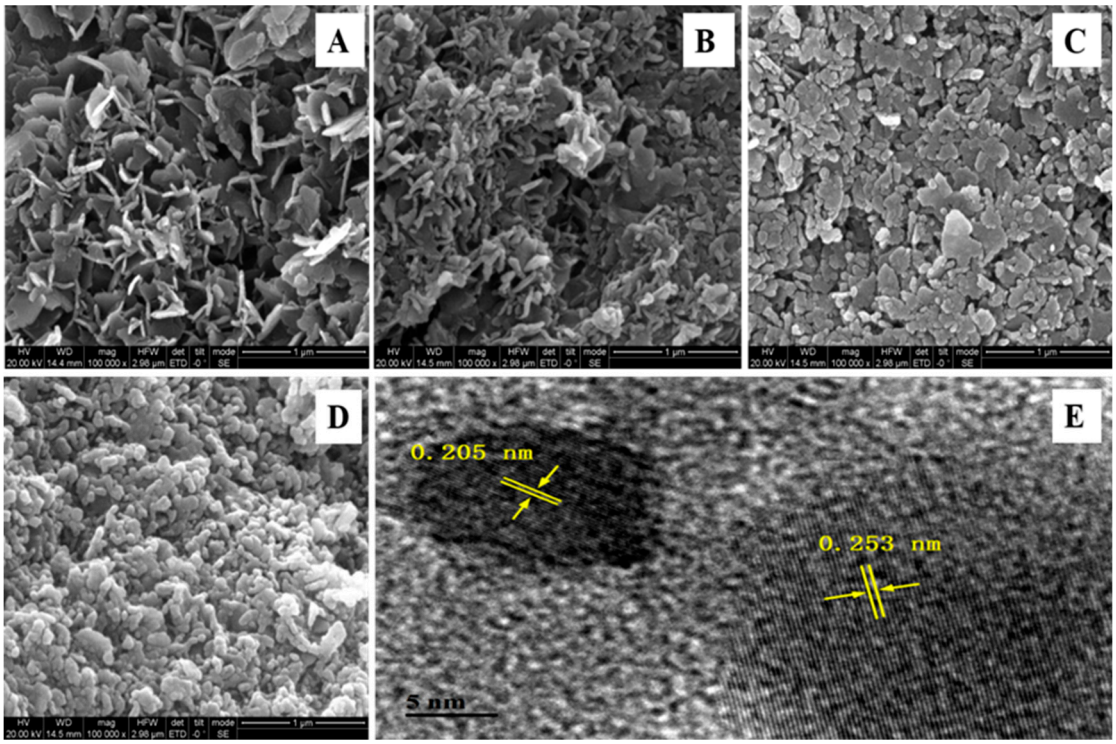

Figure 2. SEM images of the (**A**) CuMgFe-3LDH, (**B**) CuMgFe-4LDH, (**C**) CuMgFe-3LDO, and (**D**) CuMgFe-4LDO. HRTEM image of (**E**) CuMgFe-4LDO.

2.1.2. Magnetic Behavior of CuMgFe-xLDO Catalysts

The magnetic behavior of the catalysts was analyzed using VSM. All catalysts showed narrow S-shape type loops in Figure 3, indicating that all catalysts were ferromagnetic. Magnetic saturation (Ms), remanence (Mr), and coercivity (Hc) calculated from magnetically recorded data are listed in Table 1. The lower saturation magnetization and coercivity values might be due to the presence of CuO and MgO in the catalysts. The ratio of the remanence to the saturation magnetization (Mr/Ms) decreased in the following order: CuMgFe-5LDO > CuMgFe-3LDO > CuMgFe-2LDO > CuMgFe-4LDO, which was related to the inter- and intragrain exchange interactions, sub-lattice magnetization, magnetic anisotropy, and morphology of the tested sample [31]. The lower ratio corroborated its significant superparamagnetic behavior [32].

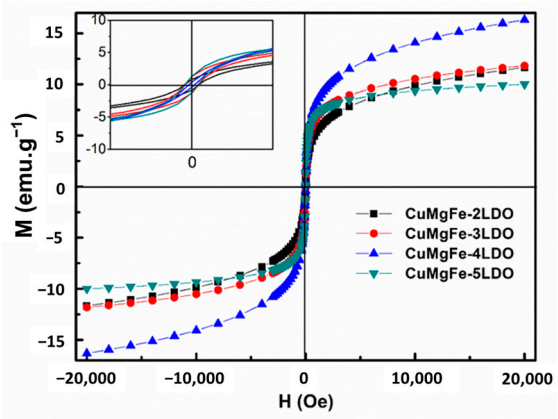

Figure 3. Magnetic hysteresis curves for the CuMgFe-xLDO catalysts.

Table 1. The magnetic properties of CuMgFe-xLDO catalysts.

Sample	M_s (emu.g^{-1})	M_r (emu.g^{-1})	M_r/M_s	H_c (Oe)
CuMgFe-2LDO	11.70	0.91	0.08	26.71
CuMgFe-3LDO	11.82	1.41	0.12	27.86
CuMgFe-4LDO	16.30	0.41	0.03	13.45
CuMgFe-5LDO	10.00	1.38	0.14	26.20

2.1.3. H_2-TPR of CuMgFe-xLDO Catalysts

The reducibility of catalysts was investigated by hydrogen temperature-programmed reduction (H_2-TPR). As shown in Figure 4, the first shoulder peak (at 205 °C, 209 °C, 191 °C, and 210 °C) in the low-temperature range for all the samples was ascribed to the reduction of CuO to Cu. The subsequent peak (at 235 °C, 242 °C, 225 °C, and 246 °C) was attributed to the reduction of $CuFe_2O_4$ to metallic Cu and Fe_2O_3 [33,34]. The third peak in the range of 300–550 °C might correspond to the transformation of Fe_2O_3 to Fe_3O_4 [35]. The peak in the high-temperature range of 550–900 °C for all the samples could be attributed to the continuous reduction of Fe_3O_4 to metallic Fe via FeO [33,36]. It should be noted that the reduction temperature of CuO in the CuMgFe-xLDO samples shifted to lower temperature compared with that of pristine CuO (around 290 °C) [33], and the reduction peak of $CuFe_2O_4$ in the CuMgFe-xLDO samples decreased significantly in comparison with that of pristine $CuFe_2O_4$ (around 340 °C) [33]. The findings indicated that the strong synergistic effect between copper and iron occurred in the CuMgFe-xLDO samples. Furthermore, the reduction peaks of CuO and $CuFe_2O_4$ in the CuMgFe-4LDO catalyst were lower than those of other catalysts, suggesting that the stronger interaction between copper and iron might occur in the CuMgFe-4LDO catalyst. Cu species could be well dispersed on the CuMgFe-4LDO catalyst surface.

2.1.4. XPS Analysis of CuMgFe-xLDO Catalysts

Cu 2p and Fe 2p spectra of CuMgFe-xLDO catalysts are shown in Figure 5a,b. A Cu $2p_{3/2}$ main peak at 933.5–933.9 eV was accompanied by a satellite peak at 942.2–942.8 eV, which was related to $CuFe_2O_4$. Additionally, all catalysts exhibited a Cu $2p_{3/2}$ peak at 931.8–931.9 eV together with a satellite peak at 940.0–940.2 eV, which could be associated with the presence of CuO. A Cu $2p_{1/2}$ main peak at 952.2–952.8 eV along with a satellite peak at 961.6–962.0 eV was also observed, in accordance with those of Cu^{2+} [37,38]. All Fe 2p spectra in Figure 5b showed two main peaks at 710.9–711.1 eV and 724.2–724.5 eV, which belonged to Fe $2p_{3/2}$ and Fe $2p_{1/2}$, respectively. Two accompanying satellite peaks at the binding energies of 718.5–718.8 eV and 732.3–732.8 eV were characteristics of Fe^{3+} cations [38–40]. Mg 1s spectra of CuMgFe-xLDO catalysts are also presented in Figure 5c. All catalysts showed a peak at 1303.5–1304.1 eV, which could be due to the presence of MgO [41].

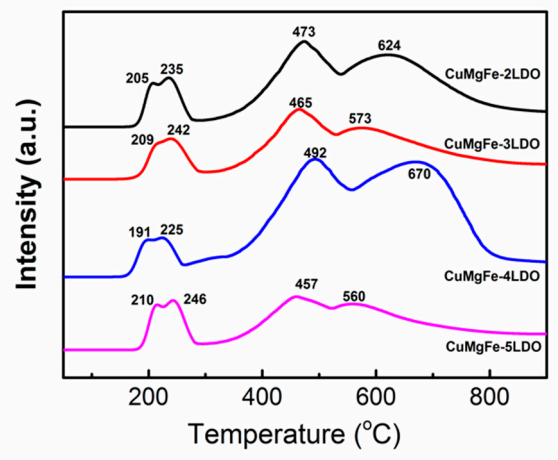

Figure 4. Hydrogen temperature-programmed reduction (H_2-TPR) profiles of CuMgFe-xLDO catalysts.

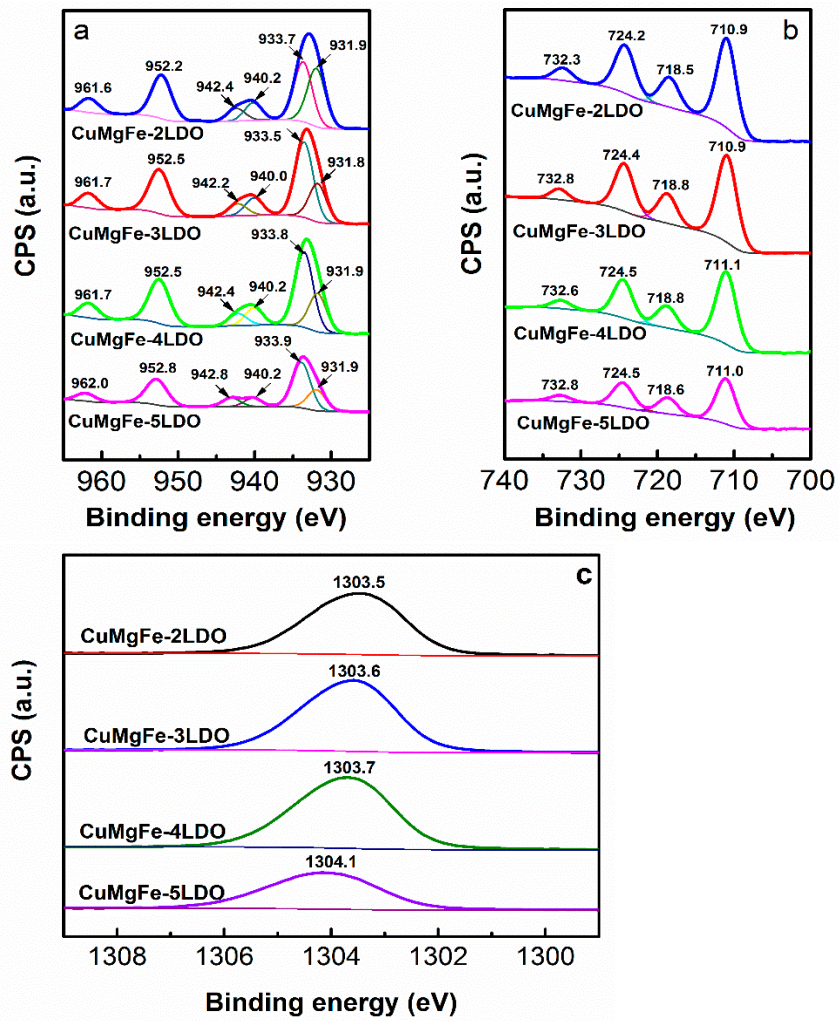

Figure 5. XPS spectra of (**a**) Cu 2p, (**b**) Fe 2p, and (**c**) Mg 1s of the CuMgFe-xLDO catalysts.

The surface element composition of CuMgFe-xLDO catalysts is summarized in Table 2. The surface Cu content and surface Cu/(Mg + Fe) atomic ratio of the CuMgFe-4LDO catalyst were slightly higher than those of the other catalysts, suggesting that Cu species could be well dispersed on the CuMgFe-4LDO catalyst. This was in line with the H_2-TPR results.

Table 2. The surface element composition and the base sites amounts of CuMgFe-xLDO catalysts.

Catalyst	Cu (mol%) [a]	Cu/(Mg + Fe) Atomic Ratio [a]	Base Sites Amounts		
			W [b] + M [b] (μmol/g)	S [b] (μmol/g)	Total Amount (μmol/g)
CuMgFe-2LDO	5.08	0.289	60.1	53.6	113.7
CuMgFe-3LDO	5.01	0.290	84.2	61.4	145.6
CuMgFe-4LDO	5.26	0.325	109.0	90.5	199.5
CuMgFe-5LDO	4.92	0.278	83.9	45.6	129.5

[a] The values were calculated from XPS; [b] W: T < 200 °C; M: 200 °C < T < 400 °C; S: T > 400 °C.

2.1.5. Basicity of Reduced Catalysts

The base properties of the CuMgFe-LDO catalysts were evaluated by the adsorption of CO_2 on the basic sites. The CO_2-TPD profiles of CuMgFe-LDO catalysts are presented in Figure 6. There were two obvious desorption domains occurring at 50–400 °C and 400–700 °C for all the catalysts. The stronger the basic sites of a catalyst were, the higher the desorption temperature of CO_2 was [42]. The low-temperature peaks below 200 °C could be attributed to the desorption of CO_2 on weak basic sites, while the desorption peaks in the range of 200–400 °C could be ascribed to the desorption of CO_2 on medium basic sites. The peaks at 549–599 °C were associated with the desorption of CO_2 on strong basic sites. The weak and medium basic sites corresponded to surface OH^- and Lewis acid-base pairings, respectively, and the strong basic sites were related to the contribution of low-coordination surface O^{2-} [43–45]. Notably, the desorption temperature on strong basic sites of the CuMgFe-4LDO catalyst was significantly higher than those of the other catalysts. It has been reported that dehydrogenation of glycerol leads to glyceraldehyde and it subsequently dehydrates to hydroxyacrolein on basic sites of the catalyst [46]. The strongest basic sites on the CuMgFe-4LDO catalyst might enhance its catalytic performance. As shown in Table 2, the total amount of basic sites decreased in the following order: CuMgFe-4LDO > CuMgFe-3LDO > CuMgFe-5LDO > CuMgFe-2LDO, indicating that the total amount of basic sites of the catalyst increased with the moderate increase of (Cu + Mg)/Fe molar ratio. Conversely, excessive (Cu + Mg)/Fe molar ratio decreased significantly the contribution of medium and strong basic sites, and thereby reducing the total amount of basic sites of the CuMgFe-5LDO catalyst. This could be associated with the morphology, crystal plane, and crystal size of MgO in the CuMgFe-5LDO catalyst. Li et al. found that MgO (100) surface primarily ended with alternant Mg^{2+}/O^{2-} ions providing medium basic sites, while MgO (111) surface primarily ended with O^{2-} ions providing strong basic sites [47]. It was reported by Marianou et al. that the basicity of MgOs was strongly affected by the morphology, texture, and chemical composition of the materials [48]. Samples with smaller crystal size and higher surface area exhibited a higher total number of basic sites [48].

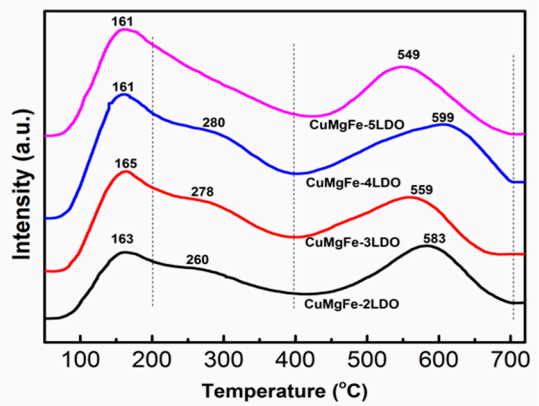

Figure 6. CO_2-TPD patterns of the reduced CuMgFe-xLDO catalysts.

2.1.6. H_2-TPD of Reduced Catalysts

H_2-TPD profiles of the CuMgFe-xLDO catalysts are shown in Figure 7. In the range of 50–700 °C, the desorption of H_2 might be assigned to three different H species. The desorption peak at low temperature (50–350 °C, H_α) might be attributed to hydrogen desorption from Cu sites. The desorption peak at high temperature (350–700 °C, H_β, H_γ) could correspond to the hydrogen desorption from two different Fe sites. Apparently, the CuMgFe-4LDO catalyst exhibited the highest H_α desorption peak temperature, indicating that a stronger metal-hydrogen interaction occurred on the surface of the CuMgFe-4LDO catalyst. This could be due to the high Cu dispersion in the CuMgFe-4LDO catalyst, which afforded more unsaturated coordination centers for the hydrogen adsorption [33]. It has been reported that enhanced H_2 activation ability could improve the activity for glycerol hydrogenolysis [24].

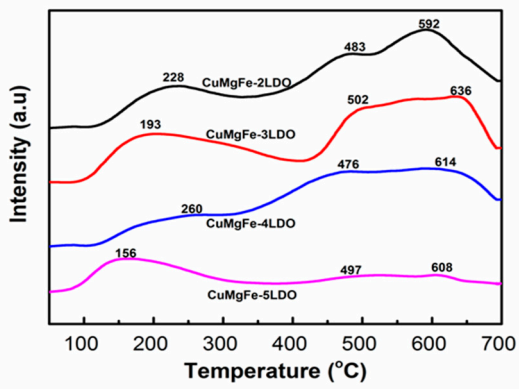

Figure 7. H_2-TPD profiles of the CuMgFe-xLDO catalysts.

2.2. Hydrogenolysis of Glycerol

2.2.1. Effect of (Cu + Mg)/Fe Molar Ratio on Catalytic Performance of Reduced CuMgFe-xLDO Catalysts

The conversions of glycerol over CuMgFe-xLDO catalysts for the hydrogenolysis of glycerol are summarized in Table 3. With the increase in (Cu + Mg)/Fe molar ratios from 2 to 4, the conversion of glycerol increased from 38.0% to 47.8%. On the contrary, the conversion of glycerol over the CuMgFe-5LDO catalyst decreased. The CuMgFe-4LDO catalyst exhibited the highest glycerol conversion and 1,2-PDO selectivity among all the catalysts.

Table 3. Hydrogenolysis of glycerol on reduced CuMgFe-xLDO catalysts [a].

Catalyst	Conversion (%)	Selectivity	
		1,2-PDO (%)	Others (%) [b]
CuMgFe-2LDO	38.0	96.9	3.1
CuMgFe-3LDO	41.3	97.0	3.0
CuMgFe-4LDO	47.8	97.5	2.5
CuMgFe-5LDO	37.5	96.2	3.4

[a] Reaction conditions: 8.0 g 75% glycerol solution, 2.0 MPa H_2, 180 °C, 10 h, 0.60 g reduced catalyst. [b] Ethylene glycol, methanol, ethanol, and 1-propanol.

According to the reaction mechanism from glycerol to 1,2-PDO proposed by Montassier [49], first, dehydrogenation of glycerol on copper would form glyceraldehyde in equilibrium with its enolic tautomer. Then, a nucleophilic reaction of water or adsorbed OH species led to a dehydroxylation reaction. Subsequently, 1,2-PDO was formed by hydrogenation of the intermediate unsaturated aldehyde (2-hydroxy acrolein). Therefore, it can be concluded that the hydrogenolysis of glycerol to 1,2-PDO needs both metal sites for activation of hydrogen and base sites for dehydration. The higher hydrogenolysis activity

over CuMgFe-4LDO catalyst might be due to the following factors. Primarily, the increase in the surface Cu content might be a factor in improving the hydrogenolysis activity of glycerol (Table 2). Furthermore, compared with the other catalysts, the stronger basic sites and the higher amount of basicity (Figure 6 and Table 2) on the CuMgFe-4LDO catalyst favored dehydration reaction of glyceraldehyde and its enolic tautomer. Consequently, the intermediate unsaturated aldehyde (2-hydroxy acrolein) was formed. Finally, on the basis of the H_2-TPD results (Figure 7), enhancing H_2 activation on Cu metal sites accelerated hydrogenation of intermediate unsaturated aldehyde (2-hydroxy acrolein), thereby improving the selectivity to 1,2-PDO.

2.2.2. Hydrogenolysis of Glycerol on Reduced CuMgFe-4LDO Catalyst at Different Temperatures

The activity of CuMgFe-4LDO catalyst for hydrogenolysis of glycerol at different temperatures is summarized in Table 4. The conversion of glycerol increased significantly from 47.8% (at 180 °C) to 75.3% (at 200 °C), suggesting that glycerol hydrogenolysis accelerated with increasing reaction temperature. Nevertheless, the selectivity to 1,2-PDO declined slightly from 97.5% (at 180 °C) to 96.5% (at 200 °C), indicating that no obvious cleavage of C–C bonds over CuMgFe-4LDO catalyst occurred even at higher temperatures.

Table 4. Hydrogenolysis of glycerol on reduced CuMgFe-4LDO catalyst at different temperatures [a].

Temperature (°C)	Conversion (%)	Selectivity	
		1, 2-PDO (%)	Others (%) [b]
180	47.8	97.5	2.5
190	60.5	97.2	2.8
200	75.3	96.5	3.5

[a] Reaction conditions: 8.0 g 75% glycerol solution, 2.0 MPa H_2, 10 h, 0.60 g reduced catalyst. [b] Ethylene glycol, methanol, ethanol, and 1-propanol.

2.2.3. Recycled Usage of Reduced CuMgFe-4LDO Catalyst

The recycling procedure of the CuMgFe-4LDO catalyst was performed for examining the stability of the catalyst. The spent catalysts were separated by an external magnetic field. Due to the magnetism for CuMgFe-4LDO catalysts, the catalysts could be easily recycled, as shown in Figure 8. The activity of recycled CuMgFe-4LDO catalyst is summarized in Table 5. The conversion of glycerol decreased slightly from 47.8% (of the fresh catalyst) to 46.9% (in the second recycle), and then it remained stable (in the third and the fourth recycles). After five times of recycling, the conversion of glycerol over the CuMgFe-4LDO catalyst decreased by 3.5%. No apparent weight loss of catalysts was observed after five times recycles.

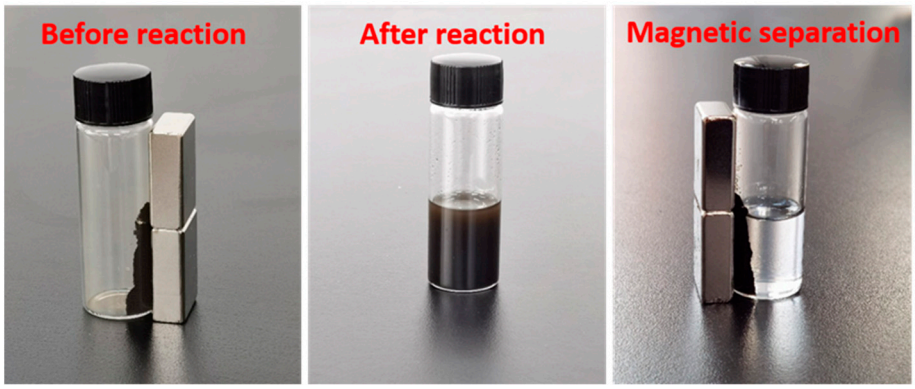

Figure 8. Images of magnetic characteristics and magnetic separation for reduced CuMgFe-4LDO catalyst.

Table 5. Hydrogenolysis of glycerol and composition on recycled CuMgFe-4LDO [a].

Recycles	Conversion (%)	Selectivity		Composition [c]		
		1, 2-PDO (%)	Others [b] (%)	Cu (mol %)	Mg (mol %)	Fe (mol %)
1	47.8	97.5	2.5	7.23	72.98	19.79
2	46.9	97.4	2.6	–	–	–
3	46.6	97.3	2.7	–	–	–
4	46.1	97.4	2.6	–	–	–
5	44.3	97.2	2.8	7.15	73.85	19.00

[a] Reaction conditions: 8.0 g 75% glycerol solution, 2.0 MPa H_2, 180 °C, 10 h, 0.60 g catalyst. [b] Ethylene glycol, methanol, ethanol, and 1-propanol. [c] the values were determined by induced coupled plasma-optical emission spectroscopy (ICP–OES).

To explore the reasons for activity loss, the compositions of the reduced catalyst and five-times-recycled catalyst were determined by induced coupled plasma-optical emission spectroscopy (ICP–OES). No obvious leaching Cu was observed after five recycles (Table 5). Meanwhile, to confirm further no Cu leaching, the catalyst was filtered off after 5 h reaction (halfway through the reaction) in the fifth recycle. At this moment, glycerol conversion and the selectivity to 1,2-propanediol were 28.5% and 97.0%, respectively. Then, the filtrate was transferred to a 100 mL stainless steel autoclave. Moreover, hydrogenolysis of glycerol was still performed under no catalyst conditions. Once more, after 5 h reaction, glycerol conversion and the selectivity to 1,2-propanediol did not further increase, indicating that no Cu leached into the filtrate. Furthermore, the XRD results of the reduced catalyst and five-times-recycled catalyst were also analyzed (Figure S1), Cu metal sizes were calculated from the diffraction peaks (220) according to the Scherrer equation. Cu metal size increased from 9.2 nm to 10.8 nm after five recycles, suggesting that the decreased activity of CuMgFe-4LDO catalyst could be due to slight sintering of copper metal.

3. Materials and Methods

3.1. Preparation of CuMgFe-Mixed Oxides Catalysts

Four CuMgFe-LDH precursors with different $(Cu^{2+} + Mg^{2+})/Fe^{3+}$ molar ratios were prepared by coprecipitation. The A solution was a 0.2 M aqueous solution containing the nitrates of Cu^{2+}, $Mg^{2+,}$ and Fe^{3+}. The B solution was an aqueous solution of NaOH and Na_2CO_3 with a concentration of 0.25 M and 0.8 M, respectively. Solution A and B were added drop-wise into the deionized water with vigorous stirring. During the coprecipitation, the slurry was kept at pH 10.0 ± 0.1 by adjusting dropping rates. The resulting suspension was aged at 60 °C for 18 h. The final precipitate was filtered, washed, and dried at 110 °C for 12 h. Layered double hydroxides were gained, and they are donated as CuMgFe-*x*LDH (*x* = 2, 3, 4 or 5 according to the $(Cu^{2+} + Mg^{2+})/Fe^{3+}$ molar ratios of 2, 3, 4, or 5). Subsequently, the hydrotalcites were calcined at 600 °C for 5 h in air, and the products are designated as CuMgFe-*x*LDO (*x* = 2, 3, 4, or 5). The nominal Cu content is 9 wt% in the CuMgFe- *x*LDO samples.

3.2. Characterization of Precursors and Catalysts

The X-ray diffraction patterns were detected on a Philips X'pert-PRO diffractometer using Cu Kα radiation (45 kV, 50 mA) (PANalytical, Etten-Leur, Nethelands).

The morphology of the CuFeMg-LDH was investigated using a Quanta 400 FEG scanning electron microscope (FEI, Hillsboro, Oregon, OR, USA) with an accelerating voltage of 20 kV.

Transmission electron microscopy (TEM) images were obtained using a Tecnai G^2 F20 transmission electron microscope (FEI, Hillsboro, Oregon, OR, USA). The samples were ultrasonically dispersed in ethanol.

The reducibility of the catalysts was studied by hydrogen temperature-programmed reduction (H_2-TPR) using a fixed-bed reactor. The catalysts were reduced under a 10% H_2/Ar mixed gas (30 mL/min) from 50 °C to 900 °C at a rate of 10 °C/min. The hydro-

gen consumption was analyzed on-line using an SC-200 gas chromatograph (Chuanyi, Chongqing, China) equipped with a thermal conductivity detector (TCD).

The X-ray photoelectron spectra (XPS) were obtained using an XSAM800 spectrometer (Kratos, Manchester, UK) with an Al Ka (hm = 1486.6 eV) X-ray source, and the binding energies were corrected using C (1 s) at 284.6 eV.

The basicity and the H_2-activation ability of the reduced catalysts were determined by temperature-programmed desorption of CO_2 and H_2 (CO_2-TPD and H_2-TPD). The catalysts were reduced at 400 °C in 10% H_2/Ar for 2 h and then cooled to 50 °C in a He flow. Subsequently, CO_2 was fed into the reactor for 0.5 h. Then the catalysts were purged at 50 °C with He for 3 h. Finally, the samples were heated linearly to 750 °C at a rate of 10 °C/min in a He flow. While the desorbed CO_2 was recorded continuously by a TCD detector. H_2-TPD was carried out by the same procedure. Only CO_2 was supplanted by the 10% H_2/Ar.

The magnetization was characterized by a superconducting quantum interference SQUID magnetometer (Quantum Design, San Diego, CA, USA) with a maximum field of 20 kOe at room temperature. The saturation magnetization (Ms), coercive force (Hc), and residual magnetization (Mr) were measured.

Chemical composition was analyzed by using an induced coupled plasma-optical emission spectroscopy (ICP–OES) analyzer (Spectro Arcos, SPECTRO Analytical Instruments GmbH, Kleve, Germany).

3.3. Catalytic Experiments

Hydrogenolysis of glycerol was performed in a 100 mL stainless steel autoclave with a mechanical stirrer and an electric temperature controller, operated under H_2 pressure of 2.0 MPa. Prior to reaction, the catalysts were reduced by 10% H_2/Ar stream at 400 °C for 2 h in a fixed-bed flowed reactor. A total of 8.0 g aqueous solution of 75 wt% glycerol and 10 wt% (based on glycerol) of the catalysts were charged into the autoclave. The liquid products were analyzed by using a Scion 456C GC gas chromatograph (Techcomp, Shanghai, China) equipped with a flame ionization detector (PEG-20M column: 30 m × 0.25 mm × 0.5 μm). The gas products were analyzed by using a Scion 456C GC gas chromatograph equipped with a thermal conductivity detector (TDX-01 column: 3 m × 3 mm).

4. Conclusions

The CuMgFe-*x*LDO catalysts derived from different (Cu + Mg)/Fe metal ratios were prepared by coprecipitation. The activity of the CuMgFe-4LDO catalyst was higher than those of other CuMgFe-*x*LDO catalysts, and the conversion of glycerol and the selectivity to 1,2-PDO reached 47.8% and 97.5% at 180 °C, respectively. The superior catalytic performance of CuMgFe-4LDO was associated with its strong basicity, excellent H_2 activation ability, and an increase in the surface Cu content. The CuMgFe-4LDO catalyst also exhibited good stability. Furthermore, the CuMgFe-*x*LDO catalysts could be easily recycled with the assistance of an external magnetic field due to their magnetism.

Supplementary Materials: The following are available online at https://www.mdpi.com/2073-4344/11/2/232/s1, Figure S1: XRD patterns of the reduced and spent CuMgFe-4LDO catalysts.

Author Contributions: Conceptualization, X.Y.; methodology, X.Y. and F.Z.; software, X.Y.; validation, X.Y.; formal analysis, X.Y.; investigation, X.Y. and F.Z.; resources, X.Y. and Y.W.; data curation, X.Y.; writing—original draft preparation, X.Y.; writing—review and editing; X.Y., F.Z., and Y.W.; supervision, X.Y.; project administration, Y.W. and D.C.; funding acquisition, X.Y. All authors have read and agreed to the published version of the manuscript.

Funding: This research was funded by the National Natural Science Foundation of China (Grant No. 21706168).

Data Availability Statement: Data presented in this study are available on request from the corresponding author.

Conflicts of Interest: The authors declare no conflict of interest.

References

1. Zope, B.N.; Hibbitts, D.D.; Neurock, M.; Davis, R.J. Reactivity of the gold/water interface during selective oxidation catalysis. *Science* **2010**, *330*, 74–78. [CrossRef]
2. Dalil, M.; Edake, M.; Sudeau, C.; Dubois, J.L.; Patience, G.S. Coke promoters improve acrolein selectivity in the gas-phase dehydration of glycerol to acrolein. *Appl. Catal. A Gen.* **2016**, *522*, 80–89. [CrossRef]
3. Yun, D.; Yun, Y.S.; Kim, T.Y.; Park, H.; Lee, J.M.; Han, J.W.; Yi, J. Mechanistic study of glycerol dehydration on Brønsted acidic amorphous aluminosilicate. *J. Catal.* **2016**, *341*, 33–43. [CrossRef]
4. Sun, D.; Yamada, Y.; Sato, S.; Ueda, W. Glycerol hydrogenolysis into useful C3 chemicals. *Appl. Catal. B Environ.* **2016**, *193*, 75–92. [CrossRef]
5. Wang, C.; Jiang, H.; Chen, C.; Chen, R.; Xing, W. Solvent effect on hydrogenolysis of glycerol to 1,2-propanediol over Cu–ZnO catalyst. *Chem. Eng. J.* **2015**, *264*, 344–350. [CrossRef]
6. Dam, J.T.; Hanefeld, U. Renewable chemicals: Dehydroxylation of glycerol and polyols. *ChemSusChem* **2011**, *4*, 1017–1034.
7. Wang, Y.; Zhou, J.; Guo, X. Catalytic hydrogenolysis of glycerol to propanediols: A review. *RSC Adv.* **2015**, *5*, 74611–74628. [CrossRef]
8. Yuan, Z.; Wang, L.; Wang, J.; Xia, S.; Chen, P.; Hou, Z.; Zheng, X. Hydrogenolysis of glycerol over homogenously dispersed copper on solid base catalysts. *Appl. Catal. B Environ.* **2011**, *101*, 431–440. [CrossRef]
9. Mane, R.; Patil, S.; Shirai, M.; Rayalu, S.; Rode, C. Influence of carbon based supports on selectivity behavior of diols and pro panol in Ru catalyzed glycerol hydrogenolysis. *Appl. Catal. B Environ.* **2017**, *204*, 134–146. [CrossRef]
10. Balaraju, M.; Rekha, V.; Prabhavathi Devi, B.L.A.; Prasad, R.B.N.; Sai Prasad, P.S.; Lingaiah, N. Surface and structural proper ties of titania-supported Ru catalysts for hydrogenolysis of glycerol. *Appl. Catal. A Gen.* **2010**, *384*, 107–114. [CrossRef]
11. Zhou, W.; Zhao, Y.; Wang, S.; Ma, X. The effect of metal properties on the reaction routes of glycerol hydrogenolysis over platinum and ruthenium catalysts. *Catal. Today* **2017**, *298*, 2–8. [CrossRef]
12. Furikado, I.; Miyazawa, T.; Koso, S.; Shimao, A.; Kunimori, K.; Tomishige, K. Catalytic performance of Rh/SiO_2 in glycerol reaction under hydrogen. *Green Chem.* **2007**, *9*, 582–588. [CrossRef]
13. Shinmi, Y.; Koso, S.; Kubota, T.; Nakagawa, Y.; Tomishige, K. Modification of Rh/SiO_2 catalyst for the hydrogenolysis of glycerol in water. *Appl. Catal. B Environ.* **2010**, *94*, 318–326. [CrossRef]
14. Rodrigues, R.; Isoda, N.; Gonçalves, M.; Figueiredo, F.C.A.; Mandelli, D.; Carvalho, W.A. Effect of niobia and alumina as support for Pt catalysts in the hydrogenolysis of glycerol. *Chem. Eng. J.* **2012**, *198–199*, 457–467. [CrossRef]
15. Zhou, W.; Zhao, Y.; Wang, Y.; Wang, S.; Ma, X. Glycerol hydrogenolysis to 1,3-propanediol on tungstate/zirconia-supported platinum: Hydrogen spillover facilitated by Pt(111) Formation. *ChemCatChem* **2016**, *8*, 3663–3671. [CrossRef]
16. Xiao, Z.; Wang, X.; Xiu, J.; Wang, Y.; Williams, C.T.; Liang, C. Synergetic effect between Cu° and Cu+ in the Cu-Cr catalysts for hydrogenolysis of glycerol. *Catal. Today* **2014**, *234*, 200–207. [CrossRef]
17. Feng, Y.; Yin, H.; Wang, A.; Shen, L.; Yu, L.; Jiang, T. Gas phase hydrogenolysis of glycerol catalyzed by Cu/ZnO/MOx (MOx = Al_2O_3, TiO_2, and ZrO_2) catalysts. *Chem. Eng. J.* **2011**, *168*, 403–412. [CrossRef]
18. Hou, M.; Jiang, H.; Liu, Y.; Chen, R. Role of initial water content in glycerol hydrogenolysis to 1,2-propanediol over Cu–ZnO catalyst. *Reac. Kinet. Mech. Cat.* **2017**, *122*, 1129–1143. [CrossRef]
19. Vila, F.; López Granados, M.; Ojeda, M.; Fierro, J.L.G.; Mariscal, R. Glycerol hydrogenolysis to 1,2-propanediol with $Cu/\gamma\text{-}Al_2O_3$: Effect of the activation process. *Catal. Today* **2012**, *187*, 122–128. [CrossRef]
20. Huang, Z.; Liu, H.; Cui, F.; Zuo, J.; Chen, J.; Xia, C. Effects of the precipitation agents and rare earth additives on the structure and catalytic performance in glycerol hydrogenolysis of Cu/SiO_2 catalysts prepared by precipitation-gel method. *Catal. Today* **2014**, *234*, 223–232. [CrossRef]
21. Zhu, S.; Gao, X.; Zhu, Y.; Zhu, Y.; Zheng, H.; Li, Y. Promoting effect of boron oxide on Cu/SiO_2 catalyst for glycerol hydrogenolysis to 1,2-propanediol. *J. Catal.* **2013**, *303*, 70–79. [CrossRef]
22. Yuan, Z.; Wang, J.; Wang, L.; Xie, W.; Chen, P.; Hou, Z.; Zheng, X. Biodiesel derived glycerol hydrogenolysis to 1,2-propanediol on Cu/MgO catalysts. *Bioresour. Technol.* **2010**, *101*, 7088–7092. [CrossRef] [PubMed]
23. Pandhare, N.N.; Pudi, S.M.; Biswas, P.; Sinha, S. Selective hydrogenolysis of glycerol to 1,2-propanediol over highly active and stable Cu/MgO catalyst in the vapor phase. *Org. Process Res. Dev.* **2016**, *20*, 1059–1067. [CrossRef]
24. Xia, S.; Nie, R.; Lu, X.; Wang, L.; Chen, P.; Hou, Z. Hydrogenolysis of glycerol over $Cu_{0.4}/Zn_{5.6-x}MgxAl_2O_{8.6}$catalysts: The role of basicity and hydrogen spillover. *J. Catal.* **2012**, *296*, 1–11. [CrossRef]
25. Xia, S.; Zheng, L.; Nie, R.; Chen, P.; Lou, H.; Hou, Z. Trivalent metal ions M^{3+} in $M_{0.02}Cu_{0.4}Mg_{5.6}Al_{1.98}(OH)_{16}CO_3$ layered double hydroxide as catalyst precursors for the hydrogenolysis of glycerol. *Chin. J. Catal.* **2013**, *34*, 986–992. [CrossRef]
26. Xia, S.; Yuan, Z.; Wang, L.; Chen, P.; Hou, Z. Hydrogenolysis of glycerol on bimetallic Pd-Cu/solid-base catalysts prepared via layered double hydroxides precursors. *Appl. Catal. A Gen.* **2011**, *403*, 173–182. [CrossRef]
27. Mondal, S.; Janardhan, R.; Lal Meena, M.; Biswas, P. Highly active Cu-Zn-Mg-Al-O catalyst derived from layered double hydroxides (LDHs) precursor for selective hydrogenolysis of glycerol to 1,2-propanediol. *J. Environ. Chem. Eng.* **2017**, *5*, 5695–5706. [CrossRef]

28. Geng, G.; Wei, R.; Liang, T.; Zhou, M.; Xiao, G. Hydrogenolysis of glycerol to propanediols on Cu–Ca–Al hydrotalcites derived catalysts. *Reac. Kinet. Mech. Catal.* **2016**, *117*, 239–251. [CrossRef]
29. Fan, G.; Li, F. Effect of sodium borohydride on growth process of controlled flower-like nanostructured Cu_2O/CuO films and their hydrophobic property. *Chem. Eng. J.* **2011**, *167*, 388–396. [CrossRef]
30. Peng, S.; Li, L.; Srinivasan, M. Electrospun $CuFe_2O_4$ nanotubes as anodes for high-performance lithium-ion batteries. *J. Energy Chem.* **2014**, *23*, 301–307. [CrossRef]
31. Shafi, K.V.P.M.; Gedanken, A.; Prozorov, R.; Balogh, J. Sonochemical preparation and size-dependent properties of nanostructured $CoFe_2O_4$ particles. *Chem. Mater.* **1998**, *10*, 3445–3450. [CrossRef]
32. Xiao, Z.; Jin, S.; Wang, X.; Li, W.; Wang, J.; Liang, C. Preparation, structure and catalytic properties of magnetically separable Cu-Fe catalysts for glycerol hydrogenolysis. *J. Mater. Chem.* **2012**, *22*, 16598–16605. [CrossRef]
33. Gao, W.; Zhao, Y.; Liu, J.; Huang, Q.; He, S.; Li, C.; Zhao, J.; Wei, M. Catalytic conversion of syngas to mixed alcohols over CuFe-based catalysts derived from layered double hydroxides. *Catal. Sci. Technol.* **2013**, *3*, 1324–1332. [CrossRef]
34. Oar-Arteta, L.; Remiro, A.; Vicente, J.; Aguayo, A.T.; Bilbao, J.; Gayubo, A.G. Stability of $CuZnOAl_2O_3$/HZSM-5 and $CuFe_2O_4$/HZSM-5 catalysts in dimethyl ether steam reforming operating in reaction–regeneration cycles. *Fuel Process. Technol.* **2014**, *126*, 145–154. [CrossRef]
35. Lin, X.; Zhang, Y.; Yin, L. Effect of various precipitants on activity and thermal stability of $CuFe_2O_4$ water-gas shift catalysts. *J. Fuel Chem. Technol.* **2014**, *42*, 1087–1092. [CrossRef]
36. Sun, Y.; Tao, L.; You, T.; Li, C.; Shan, H. Effect of sulfation on the performance of Fe_2O_3/Al_2O_3 catalyst in catalytic dehydrogenation of propane to propylene. *Chem. Eng. J.* **2014**, *244*, 145–151. [CrossRef]
37. Zhang, Q.; Wang, H.; Ning, P.; Song, Z.; Liu, X.; Duan, Y. In situ DRIFTS studies on CuO-Fe_2O_3 catalysts for low temperature selective catalytic oxidation of ammonia to nitrogen. *Appl. Surf. Sci.* **2017**, *419*, 733–743. [CrossRef]
38. Shi, X.; Chu, B.; Wang, F.; Wei, X.; Teng, L.; Fan, M.; Li, B.; Dong, L.; Dong, L. Mn-modified CuO, $CuFe_2O_4$ and γ-Fe_2O_3 three-phase strong synergistic coexistence catalyst system for NO reduction by CO with wider active window. *ACS Appl. Mater. Interfaces* **2018**, *10*, 40509–40522. [CrossRef]
39. Faheem, M.; Jiang, X.; Wang, L.; Shen, J. Synthesis of Cu_2O–$CuFe_2O_4$ microparticles from Fenton sludge and its application in the Fenton process: The key role of Cu_2O in the catalytic degradation of phenol. *RSC Adv.* **2018**, *8*, 5740–5748. [CrossRef]
40. Karim, K.M.R.; Tarek, M.; Ong, H.R.; Abdullah, H.; Yousuf, A.; Cheng, C.K.; Khan, M.M.R. Photoelectrocatalytic reduction of carbon dioxide to methanol using $CuFe_2O_4$ modified with graphene oxide under visible light irradiation. *Ind. Eng. Chem. Res.* **2019**, *58*, 563–572. [CrossRef]
41. Dubecký, F.; Kindl, D.; Hubík, P.; Mičušík, M.; Dubecký, M.; Boháček, P.; Vanko, G.; Gombia, E.; Nečas, V.; Mudroň, J. A comparative study of Mg and Pt contacts on semi-insulating GaAs: Electrical and XPS characterization. *Appl. Surf. Sci.* **2017**, *395*, 131–135. [CrossRef]
42. Li, W.H.; Sun, Y.H. Surface properties and CO adsorption on zirconia polymorphs. *J. Mol. Catal. A Chem.* **2005**, *227*, 119–124.
43. Coleman, L.J.I.; Epling, W.; Hudgins, P.R.; Croiset, E. Ni/Mg–Al mixed oxide catalyst for the steam reforming of ethanol. *Appl. Catal. A Gen.* **2009**, *363*, 52–63. [CrossRef]
44. Yu, X.; Wang, N.; Chu, W.; Liu, M. Carbon dioxide reforming of methane for syngas production over La-promoted NiMgAl catalysts derived from hydrotalcites. *Chem. Eng. J.* **2012**, *209*, 623–632. [CrossRef]
45. Wang, Y.; Li, H.; Li, X.; Chen, D.; Xiao, W. An effective iron catalyst supported on mixed MgO-Al_2O_3 for Fischer-Tropsch synthesis to olefins. *Ind. Eng. Chem. Res.* **2020**, *59*, 11462–11474. [CrossRef]
46. Balaraju, M.; Jagadeeswaraiah, K.; Sai Prasad, P.S.; Lingaiah, N. Catalytic hydrogenolysis of biodiesel derived glycerol to 1,2-propanediol over Cu–MgO catalysts. *Catal. Sci. Technol.* **2012**, *2*, 1967–1976. [CrossRef]
47. Li, S.; Lv, S.; Zhang, Y.; Li, J.; Liu, Z.; Wang, L. Syngas-derived olefins over iron-based catalysts: Effects of basic properties of MgO nanocrystals. *J. Fuel Chem. Technol.* **2018**, *46*, 1342–1351. [CrossRef]
48. Marianou, A.A.; Michailof, C.M.; Ipsakis, D.K.; Karakoulia, S.A.; Kalogiannis, K.G.; Yiannoulakis, H.; Triantafyllidis, K.S.; Lappas, A.A. Isomerization of glucose into fructose over natural and synthetic MgO catalysts. *ACS Sustain. Chem. Eng.* **2018**, *6*, 16459–16470. [CrossRef]
49. Montassier, C.; Giraud, D.; Barbier, J. Polyol conversion by liquid phase heterogeneous catalysis over metals. *Stud. Sur. Sci. Catal.* **1988**, *41*, 165–170.